Altered gene expression related to fuel use and sensory capacity in tanycytes throughout the hibernation season in the golden hamster

Vebjørn J. Melum, Béatrice Bothorel, Marie-Azélie Moralia, Valérie Simonneaux, David G Hazlerigg, Shona H Wood

Canadian Science Publishing | Canadian Journal of Zoology

Altered gene expression related to fuel use and sensory capacity in tanycytes throughout the hibernation season in the golden hamster

Journal:	*Canadian Journal of Zoology*
Manuscript ID	cjz-2024-0180.R2
Manuscript Type:	Research Article
Date Submitted by the Author:	27-Mar-2025
Complete List of Authors:	Melum, Vebjørn; UiT The Arctic University of Norway, Arctic Seasonal Timekeeping Initiative (ASTI), Arctic Chronobiology and Physiology research group, Department of Arctic and Marine Biology; University of Strasbourg, Institute of Cellular and Integrative Neurosciences Bothorel, Béatrice; University of Strasbourg, Institute of Cellular and Integrative Neurosciences Moralia, Marie-Azélie; University of Strasbourg, Institute of Cellular and Integrative Neurosciences Simonneaux, Valerie; University of Strasbourg, Institute of Cellular and Integrative Neurosciences Hazlerigg, David; UiT The Arctic University of Norway, Arctic Seasonal Timekeeping Initiative (ASTI), Arctic Chronobiology and Physiology research group, Department of Arctic and Marine Biology Wood, Shona; UiT The Arctic University of Norway, Arctic Seasonal Timekeeping Initiative (ASTI), Arctic Chronobiology and Physiology research group, Department of Arctic and Marine Biology
Is the manuscript for consideration in a Special Issue or Collection?:	17th International Hibernation Symposium Collection
Keyword:	tanycyte, hibernation, torpor, seasonal, photoperiod, refractory, Mesocricetus auratus

Altered gene expression related to fuel use and sensory capacity in tanycytes throughout the hibernation season in the golden hamster

Vebjørn. J. Melum[1,2], Béatrice Bothorel[2], Marie-Azélie Moralia[2], Valérie Simonneaux[2], David G. Hazlerigg[1], Shona H. Wood[1]

1 UiT — The Arctic University of Norway, Department of Arctic and Marine Biology, Arctic Chronobiology and Physiology research group, Tromsø, Norway

2 University of Strasbourg, Institute of Cellular and Integrative Neurosciences, Strasbourg, France

Abstract

Hibernation is a physiological and behavioural adaptation that permits survival during periods of reduced food availability and extreme environmental temperatures. This is achieved through episodes of metabolic depression and body cooling (torpor), and subsequent rewarming (arousal), cycling between which is presumed to stem from changes in hypothalamic metabolic control. Several recent lines of evidence implicate the hypothalamic tanycytes in this phenomenon.

To investigate tanycytic changes over the hibernation season, golden hamsters (*Mesocricetus auratus* (Waterhouse, 1839)), were transferred from long photoperiod 22°C to short photoperiod (SP) 8°C, sampling animals at physiologically defined points across the hibernation season for LASER capture microdissection and RNAseq of the tanycytic region.

Our analysis revealed a marked reduction in the expression of genes linked to ciliary assembly and GPCR-signalling during the hibernation season, as well as evidence for a shift towards increased glycolytic metabolism. These aspects were all reversed in refractory animals which spontaneously ceased to express torpor after extended exposure to SP 8°C. Tanycytes sampled mid-torpor show increased expression of immediate-early genes compared to the interbout euthermic state, while genes linked to RNA processing and translation show the reverse effect. The implications of these findings for the putative involvement of tanycytes in hibernation control mechanisms are discussed.

Keywords: Tanycyte, hibernation, torpor, seasonal, photoperiod, refractory, hamster, *Mesocricetus auratus*

Introduction

Hibernation is a physiological and behavioural adaptation that permits survival during seasonal periods of energy shortage *via* a combination of pre-hibernal energy storage and hibernal metabolic depression (torpor). Ground squirrels, dormice and golden/European hamsters are examples of deep hibernators, all requiring a seasonal preparative phase to express the hibernation phenotype. Torpor during deep hibernation can reduce metabolic rate to 1% of the active state (reviewed in: (Ruf and Geiser 2015)). Animals undergoing deep hibernation repeatedly cycle between the hibernating (torpid) and the active (aroused) states for the entire hibernation season (T-A cycling). The seasonal decline in photoperiod is the primary cue used to initiate the suite of seasonal physiological changes to permit the expression of the hibernation phenotype. In a lab setting, it is possible to induce the physiological preparations for deep hibernation in golden hamsters (*Mesocricetus auratus* (Waterhouse, 1839)) by transferring them from long (LP) to short photoperiods (SP). Exposure to SP results in sexual quiescence, brown adipose tissue recruitment, moderate fattening and food caching over a period of 8 weeks (Lyman et al. 1982; Markussen et al. 2024). SP-adapted animals exposed to a reduced ambient temperature (8°C) express T-A cycling for several months (Lyman et al. 1982; Markussen et al. 2024). Finally, there is a spontaneous termination of T-A cycling concomitant with physiological preparations for the coming spring including reactivation of the gonads. This is referred to as the refractory state (Sáenz de Miera et al. 2014). Importantly, the refractory state occurs spontaneously, independent of changes in ambient temperature or photoperiod, signifying the existence of an internal timing mechanism (circannual clock), which would be an advantage to an animal isolated in a hibernaculum (Gwinner 1986; Hut et al. 2014; Sáenz de Miera et al. 2014). Golden hamsters are defined as a type I circannual species, meaning only the exit from the hibernation state is spontaneous, whereas the preparation for hibernation requires a declining photoperiod signal (Dunlap et al. 2004) (and reviewed in: (Hazlerigg et al.

2023)). Hence, we may in summary identify 3 key regulatory aspects governing the hibernation season: (i) The regulation of the preparative events to allow entry into torpor and subsequent rounds of T-A cycling, (ii) the regulation of the T-A cycle itself, and (iii) the termination of the hibernation season through the development of the refractory state.

Recent studies in mammals suggest that a specialised glial cell type present in the ependymal region surrounding the third ventricle in the mediobasal hypothalamus, the tanycyte, may play a key role in all the above aspects. Tanycytes sit in a privileged position in the mediobasal hypothalamus, forming the interface between the blood brain barrier and the cerebrospinal fluid (CSF)-brain barrier. There, they are thought to act as metabolic sensors controling the access of nutrients and hormones to the brain (Parkash et al. 2015; Bolborea et al. 2020; Duquenne et al. 2021; Lhomme et al. 2021).

It has also become abundantly clear over the last two decades that tanycytes play a key role in driving seasonal photoperiodic changes in metabolic and reproductive physiology through modulation of hypothalamic thyroid hormone (TH) availability (reviewed in: (Dardente et al. 2014, 2019; Hazlerigg and Simonneaux 2015)). This process depends on photoperiod, with melatonin duration as the primary cue used to initiate the programme of seasonally adapted physiological change. Melatonin acts via MT1 receptors in the *pars tuberalis* (PT) to control photoperiod-dependent production of the glycoprotein hormone, thyrotropin (TSH), which in turn acts on TSH receptor (TSH-R)-expressing tanycytes (Hanon et al. 2008, 2010; Sáenz de Miera et al. 2013; Wood et al. 2020). In response to LP, TSH is produced and tanycytes convert inactive thyroxine (T4) to active triiodothyronine (T3) via a deiodinase enzyme (DIO2). On SP, when TSH synthesis is inhibited, increased DIO3 reduces T3 to 3,5-diiodo-l-thyronine (T2). Infusion of TSH into the 3rd ventricle of an SP golden hamster increases Dio2 expression and restores its summer phenotype within 4-6 weeks (Klosen et al. 2013). Furthermore, experimental manipulation of TH status in Siberian hamsters (*Phodopus sungorus*, (Pallas,

1773)) revealed that a hypothyroid environment is permissive for the expression of daily torpor and that T3 manipulation can reversibly halt torpor (Murphy et al. 2012; Bank et al. 2015, 2017). Studies manipulating T3 have not been reported in a deep hibernator, but it is likely that the low TH environment within the hypothalamus and subsequent effects on the reproductive axis are permissive for hibernation (Gaston and Menaker 1967; Morin and Zucker 1978; Darrow et al. 1987).

Analyses of brain c-Fos expression pattern (a marker for cellular activation) demonstrate that in both 13-lined ground squirrels (*Ictidomys tridecemlineatus,* (Mitchill, 1821)) and in golden hamsters tanycytes show dramatic changes in activation over the T-A cycle (Bratincsák et al. 2007; Markussen et al. 2024). We have previously suggested that tanycytes, through their sensitivity to factors in the blood or cerebrospinal fluid, may mediate metabolic feedback-based initiation of the spontaneous arousal process and that the observed cellular activation during T-A cycling relates to this function (Markussen et al. 2024).

Finally, in several seasonal models, including hibernators (European hamster (*Cricetus cricetus* (Linnaeus, 1758)), Arctic ground squirrel (*Urocitellus parryii* (Richardson, 1825)) and golden hamster), it has become clear that tanycytic changes in deiodinase expression occur spontaneously with the onset of the refractory state (Revel et al. 2006; Sáenz de Miera et al. 2013, 2014; Milesi et al. 2017; Chmura et al. 2022). This suggests that, as well as regulating photoperiod-dependent preparation of winter physiology, tanycytes may also drive innately timed spontaneous termination of the winter hibernating state (Hut et al. 2014; Sáenz de Miera et al. 2014).

Based upon these studies implicating tanycytes in the regulation of hibernation, the aim of this study was to characterise changes in tanycyte characteristics over the course of the hibernation season. For this purpose, we chose the golden hamster as a model, since all three aspects of hibernation regulation (photoperiodic induction, T-A cycling and the refractory state) are

strongly expressed in this species. Here, we describe changing characteristics at the transcriptome level based on RNAseq analysis of LASER capture microdissected tissue samples taken before, during and after the hibernation phase as well as from torpid and aroused animals in the middle of the hibernation phase.

Materials and Methods

Animals

Three months old male golden hamsters (*Mesocricetus auratus*) were housed under long photoperiod (LP, 14 hours of light, 10 hours of dark) and an ambient temperature of 22°C. Animals had *ad libitum* access to food and water throughout the experiment and received nesting material and a wooden stick in their home cage. Three weeks prior to the experiment, under isoflurane anesthesia, an iButton (Maxim) was implanted to record body temperature. Prior to implantation iButtons were coated in 3 layers of paraffin/Elvax coating (Respironics/Mini Mitter, Bend, OR) and sterilised. Each animal was anesthetized by 3% isoflurane, surgery was performed under 3% isoflurane and 95% oxygen. The iButton was implanted in the abdominal cavity by laparotomy. At the site of laparotomy a subcutaneous injection of lidocaine mixture (lurocaine/bupivacaine, 2.5 mg/kg each) was administered. Subcutaneous injection of meloxicam (2 mg/kg) was performed while the animal is anesthetised, and following surgery meloxicam (metacam® buvable 1.5 mg / ml, dose 1 mg / kg) was added to drinking water 3 days post-surgery. Drinking was monitored in the animals post-surgery establishing that they were drinking normally.

At the start of the experiment, six groups (n = 5 to 6 per group) were kept on LP at 22°C. The LP group was sampled 16 weeks into the experiment to age match the SP animals. The remaining animals were transferred to short photoperiod (SP, 10 hours of light/14 hours of dark) at an ambient temperature of 8°C to initiate hibernation. Based on the regression of the testis we defined animals as "pre-hibernators" and sampled 4 weeks after transfer to SP (pre-hibernation), after 8 to 12 weeks of SP prior to initiating T-A cycling (late pre-hibernation). After three T-A cycles either when aroused in interbout euthermic (IBE) or in deep torpor (torpid) we sampled animals. The average IBE duration in this experiment was approximately

24 hours, animals were sampled late in their interbout euthermia phase (23 hours). The average torpor duration in this experiment was approximately 26 hours and torpid animals were sampled at their mid-point of torpor. After approximately 20 weeks of SP exposure, animals spontaneously stopped hibernating and were sampled at least 2 weeks after the last torpor bout (refractory).

For sampling, animals were anesthetised with 4% isoflurane and decapitated. The study was conducted at the Chronobiotron (CNRS- UMS 3415) in accordance with the French National Law implementing the European Communities Council Directive 2010/63/EU and the French Directive 2013-118. Animal procedures were reviewed by the local ethical committee (Comité Régional d'Éthique en Matière d'Expérimentation Animale de Strasbourg, CEEA 35) and the official authorization was given on December 2019 by la Direction Générale de la Recherche et de l'Innovation under the number APAFIS#22534-2019100822522580 v2.

Plasma samples

At euthanasia, blood was collected in tubes with heparin, inverted and wrapped in aluminium foil to protect it from light. The blood was allowed to clot for 20 minutes on ice before moved to a precooled centrifuge at 4 °C and centrifuged for 20 minutes for euthermic animals and 50 minutes for torpid animals at 2000 G. The time span was required to obtain a clear separation of plasma and blood cells in the torpid group. Plasma was collected in aliquots and stored at -80°C until further use.

Testosterone concentration in the plasma sample was measured with a competitive inhibition ELISA kit (MyBioSource, MBS2516160, USA) following manufacturer's instructions, and optical density was measured by a microplate reader (Promega Glomax explorer GM3510) at 450 nm.

Tissue collection

After decapitation, the brain was carefully removed from the skull by one operator, while another placed the animal on its belly and proceeded with tissue collection. The interscapular adipose tissue (iAT), containing both interscapular brown adipose tissue (iBAT) and interscapular subcutaneous white adipose tissue (iWAT) was removed. The iAT was weighed and visible iBAT was dissected, and the remaining iWAT was weighed. iBAT mass = iAT mass - iWAT. Testes were dissected out and weighed to confirm reproductive status.

LASER capture microdissection and RNA extraction

The brains were covered with pre-cooled OCT, snap frozen in chilled isopentane over dry ice and 95% ethanol and stored at -80°C. Each brain was cut, with a cryostat (-20^{0}C; CM3050 S, Leica Biosystems), in series of 20 µm thick sections covering the whole medio-basal hypothalamic region (Bregma -1.8 mm to -3.2 mm) and mounted on 6-8 membrane slides (415190-9081-000, Carl Zeiss) of 8 sections each. Slides were stored at - 80^{0}C until further use.

Immediately before LASER capture microdissection (LCMD), the membrane slides were stained using cresyl violet as described previously (Melum et al. 2024). When ready, the slides were transferred to the LASER micro dissector (PALM MicroBeam system, Zeiss) with the PALMRobo software (V4.8, Zeiss) and microdissection was completed within 45 minutes to minimize RNA degradation. LCMD was carried out at 10x, with the following settings: Cut energy = 42-49; Cut focus = 84; LPC Energy = 58; LPC focus = 84. To capture a tanycyte-enriched sample and minimise the amount of ependymal cells we limited the dorso-ventral extent of the area captured to two times the width of the pars tuberalis (PT) per section. Based on our previous study this measure can correct for individual animal size differences and changes in the extent of the tanycytic region as the sections cover the rostro-caudal extent (Melum et al. 2024). The width of the area captured was only two to three cell bodies thick to further enrich for tanycytes which closely line the 3rd ventricle (Supplementary Figure 1A).

While this approach will not give a pure tanycyte sample it will be greatly enriched for tanycytes compared to previous studies of this region using the entire medio-basal hypothalamus (Haugg et al. 2022). The tanycyte-enriched samples were collected on to microdissection caps (415190-9211-000, Carl Zeiss), snap frozen on dry ice and stored at -80^{0}C. The RNA was extracted from the microdissected tissue using the Qiagen all prep DNA/RNA micro kit (80284) following the supplied instructions. The RNA integrity numbers were determined by TapeStation high sensitivity RNA analysis (5067-5579, 5067-5581, 5067-5580, Agilent) and all used samples had a RNA integrity numbers (RIN) between 7 to 9.

LCMD-RNAseq, mapping and gene counts

RNA-seq library construction was performed by BGI using their standard RNAseq protocol and Illumina high seq 4000. Quality control checks and barcode removal were performed according to the BGI protocol. Approximately 35-40 million reads per sample were generated. Mapping was performed using STARaligner and the standard settings (Dobin et al. 2013). Reads were mapped to the golden hamster genome (BCM_Maur_2.0, ref.seq: GCF_017639785.1) and the annotation was provided by NCBI (GCF_017639785.1_BCM_Maur_2.0_genomic.gtf). The mapping rate was 88%. Feature counts was used to count the mapped reads to genes, using these parameters: featureCounts -p -t exon -g gene_id, on average 70% of alignments were assigned to an annotated feature.

FASTQ files and count files were deposited in GEO under this accession identifier: GSE281814

Gene expression analysis

We determined the median counts per million (CPM) across the whole experiment for each gene and applied a cut off of 10 raw counts, removing genes with a median of less than 0.5 CPM from the analysis. 16 315 genes remained representing our LCMD transcriptome, this

dataset was used in all subsequent analysis. Three samples were excluded from the RNAseq analysis because they had low read counts and/or low RIN values and formed outliers in the initial data quality PCA analysis. In the final RNAseq analysis the numbers of animals for each group analysis were $n = 6$ in Prehib; Torpid; LP and $n = 5$ in Late Prehib; IBE; Refractory. Significance in this study was defined as a false discovery rate below 0.05.

To establish that we had a tanycyte-enriched sample, as in our previous study (Melum et al. 2024), we used a single nuclei RNA-seq dataset which determined cell type specific markers for genes in the hypothalamus (Campbell et al. 2017). Using this list, we categorize the genes expressed in our dataset into cell types. We averaged the counts per million across the experiment for the genes in those specific cell type clusters and plotted the data to show cell type enrichment in our dataset (Supplementary Figure 1B).

Differential expression analysis of the RNAseq data were performed in R, with the Rstudio interface, using the EdgeR package (McCarthy et al. 2012; Chen et al. 2014; Zhou et al. 2014). In brief, a generalized linear model (GLM) analysis following the EdgeR manual was performed to determine which genes were differentially expressed between the groups. All genes with an *FDR* less than 0.05 were used in a PCA analysis using the package PCAtools (Blighe and Lun 2019). The same genes were plotted as a heatmap with five clusters (k-means) with the use of the package ComplexHeatmap (Gu et al. 2016). Enrichment analysis on each cluster was performed using ShinyGO (Ge et al. 2020) using GOterms, Kyoto encyclopedia of genes and genomes (KEGG) (Kanehisa & Goto 2000) and Reactome pathways. Fold enrichment refers to the percentage of genes in our list belonging to a specific pathway or a term, divided by the corresponding percentage in the background genome. Therefore, fold enrichment represents the over-representation of genes within a certain term or pathway, and the false discovery rate (*FDR*) is how likely this over-representation occurs by chance.

ShinyGO automatically removes redundant terms and pathways, the top terms/pathways are displayed in the figures and full results are in Supplementary Tables 2 and 4.

The package EnhancedVolcano (Blighe K, Rana S 2024) was used to make a volcano plot of genes upregulated in the IBE and Torpid states, with an *FDR* cut off of 0.05 and no log2-fold change cut off.

Other statistical analysis

Core body temperature data from iButtons (Maxim) were handled and analysed in R, with the Rstudio interface using the Tidyverse (Wickham et al. 2019) package. Graphpad prism was used to analyse and plot the mean core body temperature data, iBAT, testes mass and plasma testosterone concentration. One-way ANOVA and a Tukey test for multiple comparison was used. P value less than 0.05 were considered significant.

All scripts used to generate the figures are available in our github repository: https://github.com/ShonaWood/SeasonalTanycytes

Results

Physiological responses over the course of a short-photoperiod induced hibernation season

Our protocol for induction of a hibernation season in golden hamsters involves transferring animals from LP 22°C to SP 8°C (Figure 1A). In line with our published work, this initiates a shift towards an Autumn/Winter program, first shutting down the reproductive axis (Figure 1 A, D, E), and entering a pre-hibernation state characterised by a downward adjustment of the core-body temperature (T_b) and an increase in brown adipose tissue (BAT) (Figure 1A, B, C)(Chayama et al. 2016; Markussen et al. 2024). After approximately 8-12 weeks in SP 8°C T-A cycling commences, defined by multi-day bouts of torpor, during which T_b is close to ambient temperature (approximately 8°C), separated by spontaneous return to euthermic temperatures (interbout euthermia (IBE)) (Figure 1A). Then, after approximately 20 weeks in SP 8°C, the animals spontaneously cease to show T-A cycling and start to re-grow their testes (refractory state) (Figure 1A, D, E). The refractory state is associated with a progressive increase in T_b but this does not reach the T_b values recorded during LP (Figure 1B).

Divergent gene expression dynamics in the tanycytic region over the course of the hibernation season

To assess how changes in tanycyte characteristics mirror hibernation status, we sampled animals from LP, SP 8°C 4 weeks (pre-hibernation), SP 8°C 8-12 weeks (late pre-hibernation), during hibernation (IBE and torpid), and finally once animals had entered the refractory state (Figure 1A). Using a LASER capture microdissection (LCMD) approach, we generated tanycyte-enriched samples (Melum et al. 2024) (Figure 1F and Supplementary Figure 1A) from each of our physiologically defined groups and these were then subjected to RNAseq.

Among the euthermic animals, we found that over 15% of all detectable transcripts showed significant changes in expression (*FDR*<0.05) over the whole experiment (seasonal differentially expressed genes (DEGs) (Supplementary Table 1). Performing a PCA analysis of the seasonal DEGs, shows that 76.8%, between sample variation in gene expression was accounted for by a single principal component, resolving samples according to seasonal status (Figure 1G).

Focusing on these seasonal DEGs, we used K-means hierarchical clustering to resolve five distinctive expression profiles showing different dynamics over the course of the hibernation season (Figure 2A). Genes constituting clusters 1 (388 genes) are characterised by high expression under LP which then declines upon exposure to SP. Cluster 1 genes maintain reduced expression under SP even in the refractory state. This suggests that cluster 1 genes represent a group whose expression is primarily dependent on photoperiodic input as opposed to seasonal hibernation status. In line with this view, two canonical photoperiod-regulated genes (Aldh1a1 and Dio2 (Hanon et al. 2008, 2010; Shearer et al. 2010)) are members of cluster 1 (Figure 2B and Supplementary Table 1).

We used both Kyoto encyclopedia of genes and genomes (KEGG) and Reactome pathway analysis to gain insights into the likely functional consequences of observed changes in gene expression in clusters 1 - 5 (Supplementary table 2, Figure 2B). Cluster 1 shows strong pathway enrichment related to amino acid metabolism (3.92-fold enrichment, 0.00034 *FDR*), retinol metabolism (10.35-fold enrichment, 0.03 *FDR*), PPAR signalling pathway (7.25-fold enrichment, 6.36×10^{-5} *FDR*) and fatty acid metabolism (3.99-fold enrichment, 0.0029 *FDR*). A closer look at the PPAR pathway enriched genes (Supplementary Figure 1B) shows that lipogenesis and fatty acid transport related genes are highly expressed in LP, concurring with earlier work noting that tanycytes transport fatty acids and in combination with astrocytes regulate lipid metabolism (Hofmann et al. 2017). This pathway enrichment also reflects the

well documented direct effects of photoperiod in retinoic acid (RA) signalling in mammals (Shearer et al. 2010) (Supplementary Figure 1C).

Cluster 2 (463 genes) is defined by low expression in the pre-hibernation and hibernation animals and high expression in LP and refractory animals. This group shows strong pathway enrichment for neurotransmitter uptake in glial cells and G-protein coupled receptor (GPCR) ligand binding (Figure 2B and Supplementary Table 2), echoing our previous work describing strong photoperiodic effects on ciliation in the tanycytic region of Siberian hamsters (Melum et al. 2024). Consistent with this, we found strong enrichment of GO terms linked to ciliary function (Figure 2C and Supplementary Table 2), and the expression patterns for key cilia genes (Tubb4b, Cfap20, Cfap47) nicely demonstrate the cluster 2 expression pattern (Figure 2A).

Cluster 3 (233 genes) does not show a strong overall seasonal expression trend, but a lower expression in the mid-hibernation season (IBE) state compared to either the late-pre-hibernation state or in the refractory state (Figure 2A). This was the smallest cluster and is enriched for neurotransmitter recycling and synapse pathways (Figure 2B and Supplementary Table 2). GO term analysis also revealed genes involved in clathrin sculpted vesicles (Gad1, Gad2, Rab3a) (Supplementary Table 2 and Figure 2B), which have been proposed to be important in the communication of tanycytes to neurons (Pasquettaz et al. 2021).

Genes constituting Clusters 4 (545 genes) and 5 (566 genes) are characterised by low levels of expression in LP, which then increase upon exposure to SP and entry into the hibernation phase, before a subsequent decline in the refractory state (Figure 2A). These two clusters differ from one another in that declining expression is seen earlier in cluster 4, when animals are still undergoing T-A cycling, than in cluster 5, in which a decline in expression occurs in the refractory state (Figure 2A).

Cluster 4 shows pathway enrichment linked to mitogen-activated protein kinase (MAPK) signalling and calcium signalling as defining the pre-hibernation state (Figure 2B). The MAPK transduction pathway relates to cell growth, division and differentiation, suggesting remodelling of the tanycytic region in response to SP exposure. Consistent with this interpretation and previous descriptions of its expression dynamics in golden hamsters, Dio3 is a member of cluster 4 (Figure 2A)(Milesi et al. 2017). We also note that Slc2a5, a fructose transporter, is highly expressed in the pre-hibernation state, concomitant with a decrease in Slc2a1, a glucose transporter (Figure 2A, D and Supplementary Figure 2A). Phosphofructokinase (Pfkp), the key enzyme in glycolysis that catalyses the phosphorylation of fructose-6-phosphase is also a member of cluster 4, along with Gapdh and Eno2, all important members of the glycolysis pathway (Figure 2A, D).

Cluster 5, constituting genes whose expression is increased during the hibernation season and then decline in the refractory state, is strongly enriched for "metabolism" pathways (Figure 2B) and the GO terms relating to catabolic processes and oxidoreductase activity (Supplementary Table 2). Specifically, genes relating to the pathways; Glycine, serine and threonine metabolism and carbohydrate metabolism show increased expression in the hibernation season (Figure 2B), as do several genes linked to glycolysis (Adpgk, Tpi1, Pgk1, Pck2, Ldhd) (Figure 2D). Similarly key elements of glucose-6-phosphatase activity including catalytic subunit 3 (G6pc3), Slc37a4 (G6pt), and Adpgk, are found in cluster 5 (Figure 2A, D). We also note that glycogen phosphorylase (Pgym), which breaks down glycogen was present in cluster 5, suggesting depletion of glycogen stores in preparation for, and, during hibernation (Figure 2A, Supplementary Figure 2B), potentially to supply neurons with glucose via the G6pase system (Barahona et al. 2024).

338 *Immediate early gene expression and RNA splicing during torpor*

339 To investigate the differences in our tanycyte-enriched samples between torpid and interbout
340 euthermic states, we performed RNASeq on animals at the mid-point of torpor (average 13.3
341 hours) at a T_b of 8°C and contrasted the expression profile with that of IBE animals (Figure
342 3A). This revealed 1674 DEGs (*FDR*<0.05), 668 of which were increased during torpor (Figure
343 3B and Supplementary Table 3). We noted that a striking number of immediate early genes
344 were increased during torpor (including c-Fos, Jun, Junb, Egr1) (Figure 3B and C), with c-Fos
345 showing the most impressive induction in terms of counts per million (Figure 3C). Also,
346 amongst the most highly expressed genes during torpor were the RNA splicing/processing
347 genes; Srsf5 and Pnisr (Figure 3B), reflected in the pathway and GOterm enrichment analysis
348 which showed strong enrichment for RNA splicing (Figure 3D and Supplementary Table 4).
349 Furthermore, pathway analysis also revealed high expression of genes related to the cellular
350 response to hypoxia during torpor (Figure 3D). Wsb1, a target of HIF1, with links to glucose
351 and TH metabolism (Dentice et al. 2005; Haque et al. 2016), is increased in torpor (Figure 3C).
352 We also note a small increase of Dio3 during torpor that is mirrored by a small increase of Dio2
353 during IBE (Figure 3B).

354 By focusing on IBE, we noted Eif5, a translation initiation factor, Dyrk1b, a kinase involved in
355 double strand break repair and transcriptional silencing, Mlx, a BHLH-zip transcription factor,
356 and Kctd21, a histone deacetylase (Figure 3B, C), were among the most increased DEGs
357 (Figure 3B). GO Enrichment analysis indicated genes relating the RNA-induced silencing
358 complex (RISC) and histone methyltransferase activity were increased during IBE (Figure 3E).
359 Collectively these data suggest that translation, gene silencing via microRNAs, and epigenetic
360 regulation processes are enhanced in the interbout euthermic phase.

Discussion

Motivated by an accumulating literature indicating that tanycytes play a core role in the regulation of energy homeostasis in mammals (Bolborea and Dale 2013; Langlet 2014; Rizzoti and Lovell-Badge 2017; Prevot et al. 2018; Dali et al. 2023), and that seasonal adjustments in metabolic physiology may be initiated by changes in tanycyte function (Ebling 2014; Lewis and Ebling 2017; Ebling and Lewis 2018; Dardente et al. 2019; Melum et al. 2024), we sought in the present study to characterise changes in tanycyte phenotype across the hibernation season in the golden hamster. To this end we undertook transcriptomic profiling of LCMD samples from the tanycytic region taken at specified points during the hibernation season defined by telemetric monitoring of T_b. Based on the reasonable assumption that changes in transcriptomic profile reflect underlying changes in cellular physiology the following inferences can be drawn about changes across the season as a whole:

Firstly, among the set of seasonal DEGs, fewer than 20% (cluster 1) appear to primarily be controlled by photoperiod as opposed to seasonal status. This demonstrates that while, in the golden hamster, the initiation of the hibernation season requires SP exposure, subsequent progression through the season from pre-hibernation to the refractory state constitutes an innately driven temporal sequence of events. The presence of Dio2, Aldh1a1 and related genes in this photoperiod-regulated subset is consistent with the current consensus that nuclear hormone receptor signalling through thyroid hormone receptor (THR), retinoic acid and retinoid receptor (RAR-RXR) interactions, is central to photoperiodic triggering of changes in tanycyte function downstream of melatonin-dependent changes in TSH production by the PT (reviewed in: (Dardente et al. 2019)). The broader enrichment of this group for genes linked to amino acid and lipid metabolism is possibly an indicator of photoperiod-induced alterations of tanycyte-astrocyte communication to regulate lipid metabolism in the hypothalamus (Hofmann et al. 2017).

The second inference focuses on the larger group of DEGs that reflect the sequential seasonal state transitions (clusters 2, 4 and 5). Here, there is clear evidence for shifting metabolic fuel use within the tanycytic region, with genes linked to fructose transport and glycolytic function showing higher expression during the pre-hibernation and hibernation state compared to LP or refractory states (Figure 2D). Use of the fructose pathway and endogenous production of fructose can shift an organism towards energy conservation with decreased mitochondrial activity and enhanced glycolytic activity, potentially representing an evolutionary conserved "survival" pathway (Johnson et al. 2020). Our data are consistent with a model in which tanycytes undergo a photoperiod-driven/innately timed metabolic switch to conserve energy by shifting towards glycolysis and an enhanced use of tanycyte glycogen stores. Photoperiodic regulation of genes involved in glycogen and glucose metabolism in tanycytes of Siberian hamsters have also been reported (Nilaweera et al. 2011). This hypothesised shift in tanycyte function would reduce tanycytic energy requirements, and might enhance glucose supply to neighbouring cells via the glucose 6 phosphatase system (Barahona et al. 2024). This response can be seen as part of an organism-wide adjustment of fuel requirements to support hibernation, which is at the same time is highly tissue and brain region-specific (Williams et al. 2005; Schwartz et al. 2013; Vermillion et al. 2015).

Our third inference is that inverse to the above-mentioned changes in fuel metabolism, genes linked to the construction and function of cilia are a major feature of the seasonal DEGs. These show a marked decline in expression with the onset of the hibernation phase and then recovery to LP levels with the onset of the refractory state. Recently, we reported a similar result in juvenile Siberian hamsters, with exposure to SP during gestation and the juvenile period causing a significant reduction in the expression of ciliary gene expression and the numbers of cilia present on the ependymal surface in the basal 3rd ventricle (Melum et al. 2024). In both these studies, the described changes in ciliary gene expression are paralleled by changes in G-protein

coupled receptor (GPCR) gene expression, reflecting the role of cilia as scaffolds for cell-surface GPCRs to perform their signalling functions (reviewed in: (Schou et al. 2015)). Hence these results suggest that, in seasonal rodent species, the overwintering state may be characterised by reduced tanycytic sensitivity to signals in the CSF bathing their apical surface.

In addition to characterising transcriptomic change over the course of the hibernation season, we also compared the expression profiles of torpid and inter-bout euthermic animals. Echoing published *in situ* hybridization-based studies in golden hamsters and in hibernating ground squirrels (Bratincsák et al. 2007; Markussen et al. 2024), we saw a striking increase in the level of expression of c-Fos in the tanycytic region of torpid animals. Moreover, this effect is seen for several other well-known immediate early genes (IEGs), including Egr1, Jun and Junb. These genes have been widely used as acute markers for cellular (and especially neuronal) activation in response to stimulatory signals acting through second messengers such as intracellular calcium or cAMP (reviewed in: (Lara Aparicio et al. 2022)). IEG acute sensitivity to stimulus relies on the fact that IEG response does not depend upon synthesis of other transcriptional regulators (reviewed in: (Bahrami and Drabløs 2016)). On this basis, the most obvious interpretation of our results is that increased IEG expression in torpor represents a tanycytic response to stimulation. This raises the interesting issue of what stimuli are responsible for this effect. At the same time, we cannot exclude the possibility that the observed changes in IEG expression are a secondary consequence of changes in tanycytic protein synthesis rate due to the low temperature in the torpid state. Since IEGs exhibit negative auto-regulation through transcriptional auto-repression (Gius et al. 1990), a general suppression of protein synthesis may lead to enhanced IEG transcription. Consistent with this interpretation, global suppression of translation during torpor and the resumption of protein synthesis in the inter-bout euthermic phase has been reported in 13-lined ground squirrels (Frerichs et al. 1998; Logan et al. 2019), and in the current study the expression of the translation initiation factor,

Eif5 was suppressed during torpor. Alternatively, given the highly brain region specific pattern of c-Fos induction during T-A cycling (Bratincsák et al. 2007; Fu et al. 2021; Markussen et al. 2024; Haugg et al. 2024), a likely scenario is that the observed tanycytic IEG response represents the actions of as yet unidentified local stimuli enhanced by suppression of translation-based autoregulatory feedback. Clearly further studies to isolate candidate stimuli and test their effects on tanycytes are now warranted.

Pathway analysis of DEGs with increased expression in torpor highlights the hypoxia response and effects on the control of RNA splicing, both of which have previously been implicated in hibernation physiology (Maistrovski et al. 2012; Sano et al. 2015; Fu et al. 2021). Notably, Wsb1 a HIF1-α induced gene (reviewed in: (Haque et al. 2016)) has been linked to ubiquitination, and hence targeted degradation of DIO2 (Dentice et al. 2005; Zavacki et al. 2009). This suggests that TH metabolism may be modulated during T-A cycling by post-translational mechanisms. While exogenous T3 delivered to the hypothalamus blocks torpor in Siberian hamsters (Murphy et al. 2012; Bank et al. 2017), the equivalent experiment is yet to be conducted in a deep hibernator. Furthermore, measurement of deiodinase enzyme activity during a T-A cycle has not been done, therefore a role for TH metabolism in the regulation of the T-A cycle rather than just the overall seasonal physiology remains to be evaluated.

During IBE, the increased expression of Mlx, a BHLH-zip transcription factor, was of particular interest. Playing a crucial role in glucose homeostasis, MLX along with MLXIP translocates to the nucleus in response to high glucose-6-phosphate conditions, targeting glucose-sensitive genes for transcription (Stoltzman et al. 2008). One of these is Txnip, which prevents the uptake of glucose into the cell, thereby forming a negative feedback loop limiting the conversion to glucose to glucose-6-phosphate for glycolysis (Stoltzman et al. 2008). Expression of Txnip in the mediobasal hypothalamus (i.e. the tanycytic region) is induced in response to fasting in mice, daily torpor in Siberian hamsters (Hand et al. 2013), torpor in the garden dormouse

(*Eliomys quersinus*, (Linnaeus 1766)) (Haugg et al. 2024) and the 13-lined ground squirrel (Schwartz et al. 2013). We see no change in Txnip expression in the golden hamster tanycytes despite the up-regulation of Mlx (Supplementary table 1). Recently, it was shown that MLX sequestered to lipid droplets in the cytoplasm cannot enter the nucleus in response to glucose, preventing it from exerting transcriptional effects (Mejhert et al. 2020). Tanycytes are rich in lipid droplets (reviewed in: (Rodríguez et al. 2019)), therefore, we speculate that MLX may be sequestered to lipid droplets in the IBE phase. Since golden hamsters eat in the IBE phase, this may provide a mechanism to ensure tanycytic sequestering of glucose to support glycolysis upon re-entry to torpor.

Conclusions

While RNA profiling does not permit the drawing of firm conclusions about how tanycytic function changes over the course of the hibernation season, the data we present serve a useful hypothesis-generating function for future studies. Based on our analysis, we identify the following priorities for further research: 1) defining how tanycytic sensitivity to metabolites and other extracellular signals changes over the course of the hibernation season 2) understanding how tanycytic energy metabolism changes and the relationship between this and the function of tanycytes and neighbouring hypothalamic cells and 3) understanding the causes of the dramatic changes in tanycytic IEG expression during T-A cycling and the consequences of these for tanycytic function during torpor.

Acknowledgements

We wish to acknowledge Clarisse Quignon for her help with sample collection. We are grateful to Dominique Ciocca and Sophie Foisset Reibel for teaching animal husbandry technique. We are also grateful to all the technical staff at the chronobiotron for their support. Further, we thank Stian Olsen and Anne Grethe Hestnes for invaluable technical assistance and guidance on the LASER capture microdissection instrument. Finally, VJM would like to thank Alex C. West, Gerard Clarke and Yin-Chen Hsieh for insightful comments on an early draft of the manuscript.

Competing interests

There are no competing interests.

Funding

The work was supported by grants from the Tromsø forskningsstiftelse (TFS) starter grant TFS2016SW and the TFS infrastructure grant (IS3_17_SW) awarded to S.H.W. It was also co-funded by the European Union (ERC, HiTime, 101086671). Views and opinions expressed are however those of the author(s) only and do not necessarily reflect those of the European Union or the European Research Council. Neither the European Union nor the granting authority can be held responsible for them. The Arctic seasonal timekeeping initiative (ASTI) grant and UiT strategic funds support D.G.H. and S.H.W.

Data availability

Sequencing data generated and analyzed during this study are available in the Gene expression omnibus (GEO) repository under the accession GSE281814.

References

Bahrami, S., and Drabløs, F. 2016. Gene regulation in the immediate-early response process. Adv. Biol. Regul. **62**: 37–49. doi:10.1016/j.jbior.2016.05.001.

Bank, J.H.H., Cubuk, C., Wilson, D., Rijntjes, E., Kemmling, J., Markovsky, H., Barrett, P., and Herwig, A. 2017. Gene expression analysis and microdialysis suggest hypothalamic triiodothyronine (T3) gates daily torpor in Djungarian hamsters (Phodopus sungorus). J. Comp. Physiol. B **187**(5–6): 857–868. Springer Berlin Heidelberg. doi:10.1007/s00360-017-1086-5.

Bank, J.H.H., Kemmling, J., Rijntjes, E., Wirth, E.K., and Herwig, A. 2015. Thyroid hormone status affects expression of daily torpor and gene transcription in Djungarian hamsters (Phodopus sungorus). Horm. Behav. **75**: 120–129. Academic Press. doi:10.1016/j.yhbeh.2015.09.006.

Barahona, M.J., Ferrada, L., Vera, M., and Nualart, F. 2024. Tanycytes release glucose using the glucose-6-phosphatase system during hypoglycemia to control hypothalamic energy balance. Mol. Metab. **84**(April): 101940. The Authors. doi:10.1016/j.molmet.2024.101940.

Blighe K, Rana S, L.M. 2024. EnhancedVolcano: Publication-ready volcano plots with enhanced colouring and labeling. R package version 1.22.0.

Blighe, K., and Lun, A. 2019. PCAtools: everything Principal Components Analysis.

Bolborea, M., and Dale, N. 2013. Hypothalamic tanycytes: potential roles in the control of feeding and energy balance. Trends Neurosci. **36**(2): 91–100. Elsevier. doi:10.1016/j.tins.2012.12.008.

524 Bolborea, M., Pollatzek, E., Benford, H., Sotelo-Hitschfeld, T., and Dale, N. 2020.
525 Hypothalamic tanycytes generate acute hyperphagia through activation of the arcuate neuronal
526 network. Proc. Natl. Acad. Sci. **117**(25): 14473–14481. doi:10.1073/pnas.1919887117.

527 Bratincsák, A., McMullen, D., Miyake, S., Tóth, Z.E., Hallenbeck, J.M., and Palkovits, M.
528 2007. Spatial and temporal activation of brain regions in hibernation:c-fos expression during
529 the hibernation bout in thirteen-lined ground squirrel. J. Comp. Neurol. **505**(4): 443–458.
530 doi:10.1002/cne.21507.

531 Campbell, J.N., Macosko, E.Z., Fenselau, H., Pers, T.H., Lyubetskaya, A., Tenen, D., Goldman,
532 M., Verstegen, A.M.J., Resch, J.M., McCarroll, S.A., Rosen, E.D., Lowell, B.B., and Tsai, L.T.
533 2017. A molecular census of arcuate hypothalamus and median eminence cell types. Nat.
534 Neurosci. **20**(3): 484–496. doi:10.1038/nn.4495.

535 Chayama, Y., Ando, L., Tamura, Y., Miura, M., and Yamaguchi, Y. 2016. Decreases in body
536 temperature and body mass constitute pre-hibernation remodelling in the Syrian golden
537 hamster, a facultative mammalian hibernator. R. Soc. Open Sci. **3**(4): 160002.
538 doi:10.1098/rsos.160002.

539 Chen, Y., Lun, A.T.L., and Smyth, G.K. 2014. Differential Expression Analysis of Complex
540 RNA-seq Experiments Using edgeR. *In* Statistical Analysis of Next Generation Sequencing
541 Data. *Edited by* S. Datta and D. Nettleton. Frontiers in Probability and the Statistical Sciences.
542 Springer, Cham. doi:10.1007/978-3-319-07212-8_3

543 Chmura, H.E., Duncan, C., Saer, B., Moore, J.T., Barnes, B.M., Loren Buck, C., Christian,
544 H.C., Loudon, A.S.I., and Williams, C.T. 2022. Hypothalamic remodeling of thyroid hormone
545 signaling during hibernation in the arctic ground squirrel. Commun. Biol. **5**(1): 492.
546 doi:10.1038/s42003-022-03431-8.

547 Dali, R., Estrada-Meza, J., and Langlet, F. 2023. Tanycyte, the neuron whisperer. Physiol.
548 Behav. **263**: 114108. doi:10.1016/j.physbeh.2023.114108.

549 Dardente, H., Hazlerigg, D.G., and Ebling, F.J.P. 2014. Thyroid Hormone and Seasonal
550 Rhythmicity. Front. Endocrinol. (Lausanne). **5**: 19. Frontiers. doi:10.3389/fendo.2014.00019.

551 Dardente, H., Wood, S., Ebling, F., and Sáenz de Miera, C. 2019. An integrative view of
552 mammalian seasonal neuroendocrinology. J. Neuroendocrinol. **31**(5): e12729.
553 doi:10.1111/jne.12729.

554 Darrow, J.M., Yogev, L., and Goldman, B.D. 1987. Patterns of reproductive hormone secretion
555 in hibernating Turkish hamsters. Am J Physiol Regul Integr Comp Physiol **253**: 329–336.

556 Dentice, M., Bandyopadhyay, A., Gereben, B., Callebaut, I., Christoffolete, M.A., Kim, B.W.,
557 Nissim, S., Mornon, J.-P., Zavacki, A.M., Zeöld, A., Capelo, L.P., Curcio-Morelli, C., Ribeiro,
558 R., Harney, J.W., Tabin, C.J., and Bianco, A.C. 2005. The Hedgehog-inducible ubiquitin ligase
559 subunit WSB-1 modulates thyroid hormone activation and PTHrP secretion in the developing
560 growth plate. Nat. Cell Biol. **7**(7): 698–705. doi:10.1038/ncb1272.

561 Dobin, A., Davis, C.A., Schlesinger, F., Drenkow, J., Zaleski, C., Jha, S., Batut, P., Chaisson,
562 M., and Gingeras, T.R. 2013. STAR: ultrafast universal RNA-seq aligner. Bioinformatics
563 **29**(1): 15–21. doi:10.1093/bioinformatics/bts635.

564 Dunlap, J.C., Loros, J.J., and DeCoursey, P.J. 2004. Chronobiology: biological timekeeping.
565 Sinauer Associates. Available from https://psycnet.apa.org/record/2003-06316-000.

566 Duquenne, M., Folgueira, C., Bourouh, C., Millet, M., Silva, A., Clasadonte, J., Imbernon, M.,
567 Fernandois, D., Martinez-Corral, I., Kusumakshi, S., Caron, E., Rasika, S., Deliglia, E., Jouy,
568 N., Oishi, A., Mazzone, M., Trinquet, E., Tavernier, J., Kim, Y.-B., Ory, S., Jockers, R.,
569 Schwaninger, M., Boehm, U., Nogueiras, R., Annicotte, J.-S., Gasman, S., Dam, J., and Prévot,
570 V. 2021. Leptin brain entry via a tanycytic LepR–EGFR shuttle controls lipid metabolism and
571 pancreas function. Nat. Metab. **3**(8): 1071–1090. doi:10.1038/s42255-021-00432-5.

572 Ebling, F.J.P., and Lewis, J.E. 2018. Tanycytes and hypothalamic control of energy
573 metabolism. Glia **66**(6): 1176–1184. doi:10.1002/glia.23303.

574 Ebling, F.J.P.P. 2014. On the value of seasonal mammals for identifying mechanisms
575 underlying the control of food intake and body weight. Horm. Behav. **66**(1): 56–65. Elsevier
576 B.V. doi:10.1016/j.yhbeh.2014.03.009.

577 Frerichs, K.U., Smith, C.B., Brenner, M., DeGracia, D.J., Krause, G.S., Marrone, L., Dever,
578 T.E., and Hallenbeck, J.M. 1998. Suppression of protein synthesis in brain during hibernation
579 involves inhibition of protein initiation and elongation. Proc. Natl. Acad. Sci. **95**(24): 14511–
580 14516. doi:10.1073/pnas.95.24.14511.

581 Fu, R., Gillen, A.E., Grabek, K.R., Riemondy, K.A., Epperson, L.E., Bustamante, C.D.,
582 Hesselberth, J.R., and Martin, S.L. 2021. Dynamic RNA Regulation in the Brain Underlies
583 Physiological Plasticity in a Hibernating Mammal. Front. Physiol. **11**.
584 doi:10.3389/fphys.2020.624677.

585 Gaston, S., and Menaker, M. 1967. Photoperiodic control of hamster testis. Science (80-.).
586 **158**(3803): 925–928.

587 Ge, S.X., Jung, D., Jung, D., and Yao, R. 2020. ShinyGO: a graphical gene-set enrichment tool
588 for animals and plants. Bioinformatics **36**(8): 2628–2629. Oxford Academic.
589 doi:10.1093/BIOINFORMATICS/BTZ931.

590 Gius, D., Cao, X.M., Rauscher, F.J., Cohen, D.R., Curran, T., and Sukhatme, V.P. 1990.
591 Transcriptional activation and repression by Fos are independent functions: the C terminus
592 represses immediate-early gene expression via CArG elements. Mol. Cell. Biol. **10**(8): 4243–
593 4255. doi:10.1128/MCB.10.8.4243.

594 Gu, Z., Eils, R., and Schlesner, M. 2016. Complex heatmaps reveal patterns and correlations in
595 multidimensional genomic data. Bioinformatics **32**(18): 2847–2849.
596 doi:10.1093/bioinformatics/btw313.

597 Gwinner, E. 1986. Circannual rhythms. Springer Verlag, Berlin Heidelberg.

598 Hand, L.E., Saer, B.R.C., Hui, S.T., Jinnah, H.A., Steinlechner, S., Loudon, A.S.I., and
599 Bechtold, D.A. 2013. Induction of the metabolic regulator txnip in fasting-induced and natural
600 torpor. Endocrinology **154**(6): 2081–2091. doi:10.1210/en.2012-2051.

601 Hanon, E.A., Lincoln, G.A., Fustin, J.-M., Dardente, H., Masson-Pévet, M., Morgan, P.J., and
602 Hazlerigg, D.G. 2008. Ancestral TSH mechanism signals summer in a photoperiodic mammal.
603 Curr. Biol. **18**(15): 1147–52. doi:10.1016/j.cub.2008.06.076.

604 Hanon, E.A., Routledge, K., Dardente, H., Masson-Pévet, M., Morgan, P.J., and Hazlerigg,
605 D.G. 2010. Effect of photoperiod on the thyroid-stimulating hormone neuroendocrine system
606 in the European hamster (Cricetus cricetus). J. Neuroendocrinol. **22**(1): 51–5.
607 doi:10.1111/j.1365-2826.2009.01937.x.

608 Haque, M., Kendal, J.K., MacIsaac, R.M., and Demetrick, D.J. 2016. WSB1: from homeostasis
609 to hypoxia. J. Biomed. Sci. **23**(1): 61. doi:10.1186/s12929-016-0270-3.

610 Haugg, E., Borner, J., Diedrich, V., and Herwig, A. 2022. Comparative transcriptomics of the
611 Djungarian hamster hypothalamus during short photoperiod acclimation and spontaneous
612 torpor. FEBS Open Bio **12**(2): 443–459. doi:10.1002/2211-5463.13350.

613 Haugg, E., Borner, J., Stalder, G., Kübber-Heiss, A., Giroud, S., and Herwig, A. 2024.
614 Comparative transcriptomics of the garden dormouse hypothalamus during hibernation. FEBS
615 Open Bio **14**(2): 241–257. doi:10.1002/2211-5463.13731.

616 Hazlerigg, D., and Simonneaux, V. 2015. Seasonal reproduction in mammals. In Knobil and
617 Neill's physiology and reproduction, 4th edition. Edited by T. Plant and A. Zeleznic. Academic
618 Press. pp. 1575–1660.

619 Hazlerigg, D.G., Appenroth, D., Tomotani, B.M., West, A.C., and Wood, S.H. 2023. Biological
620 timekeeping in polar environments: lessons from terrestrial vertebrates. J. Exp. Biol. **226**(23).
621 doi:10.1242/jeb.246308.

622 Hofmann, K., Lamberz, C., Piotrowitz, K., Offermann, N., But, D., Scheller, A., Al-Amoudi,
623 A., and Kuerschner, L. 2017. Tanycytes and a differential fatty acid metabolism in the
624 hypothalamus. Glia **65**(2): 231–249. doi:10.1002/glia.23088.

625 Hut, R.A.A., Dardente, H., and Riede, S.J.J. 2014. Seasonal Timing: How Does a Hibernator
626 Know When to Stop Hibernating? Curr. Biol. **24**(13): R602–R605. Cell Press.
627 doi:10.1016/j.cub.2014.05.061.

Johnson, R.J., Stenvinkel, P., Andrews, P., Sánchez-Lozada, L.G., Nakagawa, T., Gaucher, E., Andres-Hernando, A., Rodriguez-Iturbe, B., Jimenez, C.R., Garcia, G., Kang, D.H., Tolan, D.R., and Lanaspa, M.A. 2020. Fructose metabolism as a common evolutionary pathway of survival associated with climate change, food shortage and droughts. J. Intern. Med. **287**(3): 252–262. doi:10.1111/joim.12993.

Kanehisa, M., Goto, S. 2000. KEGG: Kyoto Encyclopedia of Genes and Genomes, Nucleic Acids Res **28**(1):27–30, doi:10.1093/nar/28.1.27.

Klosen, P., Sébert, M.-E., Rasri, K., Laran-Chich, M.-P., and Simonneaux, V. 2013. TSH restores a summer phenotype in photoinhibited mammals via the RF-amides RFRP3 and kisspeptin. FASEB J. **27**(7): 2677–86. doi:10.1096/fj.13-229559.

Langlet, F. 2014. Tanycytes: A Gateway to the Metabolic Hypothalamus. J. Neuroendocrinol. **26**(11): 753–760. doi:10.1111/jne.12191.

Lara Aparicio, S.Y., Laureani Fierro, Á. de J., Aranda Abreu, G.E., Toledo Cárdenas, R., García Hernández, L.I., Coria Ávila, G.A., Rojas Durán, F., Aguilar, M.E.H., Manzo Denes, J., Chi-Castañeda, L.D., and Pérez Estudillo, C.A. 2022. Current Opinion on the Use of c-Fos in Neuroscience. NeuroSci **3**(4): 687–702. doi:10.3390/neurosci3040050.

Lewis, J.E., and Ebling, F.J.P. 2017. Tanycytes As Regulators of Seasonal Cycles in Neuroendocrine Function. Front. Neurol. **8**: 79. Frontiers. doi:10.3389/fneur.2017.00079.

Lhomme, T., Clasadonte, J., Imbernon, M., Fernandois, D., Sauve, F., Caron, E., da Silva Lima, N., Heras, V., Martinez-Corral, I., Mueller-Fielitz, H., Rasika, S., Schwaninger, M., Nogueiras, R., and Prevot, V. 2021. Tanycytic networks mediate energy balance by feeding lactate to glucose-insensitive POMC neurons. J. Clin. Invest. **131**(18). doi:10.1172/JCI140521.

650 Logan, S.M., Wu, C.-W., and Storey, K.B. 2019. The squirrel with the lagging eIF2: Global
651 suppression of protein synthesis during torpor. Comp. Biochem. Physiol. Part A Mol. Integr.
652 Physiol. **227**: 161–171. doi:10.1016/j.cbpa.2018.10.014.

653 Lyman, C.P., Willis, J.., Malan, A., and Wang, L.C.. 1982. Hibernation and torpor in mammals
654 and birds. Edited ByC.P. Lyman. Academic Press, New York.

655 Maistrovski, Y., Biggar, K.K., and Storey, K.B. 2012. HIF-1α regulation in mammalian
656 hibernators: role of non-coding RNA in HIF-1α control during torpor in ground squirrels and
657 bats. J. Comp. Physiol. B **182**(6): 849–859. doi:10.1007/s00360-012-0662-y.

658 Markussen, F.A.F., Cázarez-Márquez, F., Melum, V.J., Hazlerigg, D., and Wood, S. 2024. C-
659 Fos Induction in the Choroid Plexus, Tanycytes and Pars Tuberalis Is an Early Indicator of
660 Spontaneous Arousal From Torpor in a Deep Hibernator . J. Exp. Biol. doi:10.1242/jeb.247224.

661 McCarthy, D.J., Chen, Y., and Smyth, G.K. 2012. Differential expression analysis of
662 multifactor RNA-Seq experiments with respect to biological variation. Nucleic Acids Res.: 1–
663 10. doi:10.1093/nar/gks042.

664 Mejhert, N., Kuruvilla, L., Gabriel, K.R., Elliott, S.D., Guie, M.-A., Wang, H., Lai, Z.W., Lane,
665 E.A., Christiano, R., Danial, N.N., Farese, R. V., and Walther, T.C. 2020. Partitioning of MLX-
666 Family Transcription Factors to Lipid Droplets Regulates Metabolic Gene Expression. Mol.
667 Cell **77**(6): 1251-1264.e9. doi:10.1016/j.molcel.2020.01.014.

668 Melum, V.J., Sáenz de Miera, C., Markussen, F.A.F., Cázarez-Márquez, F., Jaeger, C., Sandve,
669 S.R., Simonneaux, V., Hazlerigg, D.G., and Wood, S.H. 2024. Hypothalamic tanycytes as
670 mediators of maternally programmed seasonal plasticity. Curr. Biol. **34**(3): 632-640.e6. Cell
671 Press. doi:10.1016/J.CUB.2023.12.042.

672 Milesi, S., Simonneaux, V., and Klosen, P. 2017. Downregulation of Deiodinase 3 is the earliest
673 event in photoperiodic and photorefractory activation of the gonadotropic axis in seasonal
674 hamsters. Sci. Rep. **7**(1): 17739. doi:10.1038/s41598-017-17920-y.

675 Morin, L.P., and Zucker, I. 1978. Photoperiodic regulation of copulatory behaviour in the male
676 hamster. J. Endocrinol. **77**(2): 249–258. J Endocrinol. doi:10.1677/JOE.0.0770249.

677 Murphy, M., Jethwa, P.H., Warner, A., Barrett, P., Nilaweera, K.N., Brameld, J.M., and Ebling,
678 F.J.P. 2012. Effects of Manipulating Hypothalamic Triiodothyronine Concentrations on
679 Seasonal Body Weight and Torpor Cycles in Siberian Hamsters. Endocrinology **153**(1): 101–
680 112. doi:10.1210/en.2011-1249.

681 Nilaweera, K., Herwig, A., Bolborea, M., Campbell, G., Mayer, C.D., Morgan, P.J., Ebling,
682 F.J.P., and Barrett, P. 2011. Photoperiodic regulation of glycogen metabolism, glycolysis, and
683 glutamine synthesis in tanycytes of the Siberian hamster suggests novel roles of tanycytes in
684 hypothalamic function. Glia **59**(11): 1695–1705. doi:10.1002/glia.21216.

685 Parkash, J., Messina, A., Langlet, F., Cimino, I., Loyens, A., Mazur, D., Gallet, S., Balland, E.,
686 Malone, S.A., Pralong, F., Cagnoni, G., Schellino, R., De Marchis, S., Mazzone, M.,
687 Pasterkamp, R.J., Tamagnone, L., Prevot, V., and Giacobini, P. 2015. Semaphorin7A regulates
688 neuroglial plasticity in the adult hypothalamic median eminence. Nat. Commun. **6**: 6385.
689 doi:10.1038/ncomms7385.

690 Pasquettaz, R., Kolotuev, I., Rohrbach, A., Gouelle, C., Pellerin, L., and Langlet, F. 2021.
691 Peculiar protrusions along tanycyte processes face diverse neural and nonneural cell types in
692 the hypothalamic parenchyma. J. Comp. Neurol. **529**(3): 553–575. doi:10.1002/cne.24965.

693 Prevot, V., Dehouck, B., Sharif, A., Ciofi, P., Giacobini, P., and Clasadonte, J. 2018. The
694 Versatile Tanycyte: A Hypothalamic Integrator of Reproduction and Energy Metabolism.
695 Endocr. Rev. **39**(3): 333–368. doi:10.1210/er.2017-00235.

696 Revel, F.G., Saboureau, M., Pévet, P., Mikkelsen, J.D., and Simonneaux, V. 2006. Melatonin
697 regulates type 2 deiodinase gene expression in the Syrian hamster. Endocrinology **147**(10):
698 4680–7. doi:10.1210/en.2006-0606.

699 Rizzoti, K., and Lovell-Badge, R. 2017. Pivotal role of median eminence tanycytes for
700 hypothalamic function and neurogenesis. Mol. Cell. Endocrinol. **445**: 7–13. Elsevier.
701 doi:10.1016/J.MCE.2016.08.020.

702 Rodríguez, E., Guerra, M., Peruzzo, B., and Blázquez, J.L. 2019. Tanycytes: A rich
703 morphological history to underpin future molecular and physiological investigations. J.
704 Neuroendocrinol. **31**(3). doi:10.1111/jne.12690.

705 Ruf, T., and Geiser, F. 2015. Daily torpor and hibernation in birds and mammals. Biol. Rev.
706 **90**(3): 891–926. doi:10.1111/brv.12137.

707 Sáenz de Miera, C., Hanon, E.A., Dardente, H., Birnie, M., Simonneaux, V., Lincoln, G.A., and
708 Hazlerigg, D.G. 2013. Circannual variation in thyroid hormone deiodinases in a short-day
709 breeder. J. Neuroendocrinol. **25**(4): 412–21. doi:10.1111/jne.12013.

710 Sáenz de Miera, C., Monecke, S., Bartzen-Sprauer, J., Laran-Chich, M.-P., Pévet, P., Hazlerigg,
711 D.G., and Simonneaux, V. 2014. A Circannual Clock Drives Expression of Genes Central for
712 Seasonal Reproduction. Curr. Biol. **24**(13): 1500–1506. doi:10.1016/j.cub.2014.05.024.

713 Sano, Y., Shiina, T., Naitou, K., Nakamori, H., and Shimizu, Y. 2015. Hibernation-specific
714 alternative splicing of the mRNA encoding cold-inducible RNA-binding protein in the hearts
715 of hamsters. Biochem. Biophys. Res. Commun. **462**(4): 322–325. Biochem Biophys Res
716 Commun. doi:10.1016/J.BBRC.2015.04.135.

717 Schou, K.B., Pedersen, L.B., and Christensen, S.T. 2015. Ins and outs of GPCR signaling in
718 primary cilia. EMBO Rep. **16**(9): 1099–1113. doi:10.15252/embr.201540530.

719 Schwartz, C., Hampton, M., and Andrews, M.T. 2013. Seasonal and Regional Differences in
720 Gene Expression in the Brain of a Hibernating Mammal. PLoS One **8**(3): e58427. Public
721 Library of Science. doi:10.1371/journal.pone.0058427.

722 Shearer, K.D., Goodman, T.H., Ross, A.W., Reilly, L., Morgan, P.J., and McCaffery, P.J. 2010.
723 Photoperiodic regulation of retinoic acid signaling in the hypothalamus. J. Neurochem. **112**(1):
724 246–257. doi:10.1111/j.1471-4159.2009.06455.x.

725 Stoltzman, C.A., Peterson, C.W., Breen, K.T., Muoio, D.M., Billin, A.N., and Ayer, D.E. 2008.
726 Glucose sensing by MondoA:Mlx complexes: A role for hexokinases and direct regulation of
727 thioredoxin-interacting protein expression. Proc. Natl. Acad. Sci. **105**(19): 6912–6917.
728 doi:10.1073/pnas.0712199105.

729 Vermillion, K.L., Anderson, K.J., Hampton, M., and Andrews, M.T. 2015. Gene expression
730 changes controlling distinct adaptations in the heart and skeletal muscle of a hibernating
731 mammal. Physiol. Genomics **47**(3): 58–74. doi:10.1152/physiolgenomics.00108.2014.

732 Wickham, H., Averick, M., Bryan, J., Chang, W., McGowan, L., François, R., Grolemund, G.,
733 Hayes, A., Henry, L., Hester, J., Kuhn, M., Pedersen, T., Miller, E., Bache, S., Müller, K.,
734 Ooms, J., Robinson, D., Seidel, D., Spinu, V., Takahashi, K., Vaughan, D., Wilke, C., Woo, K.,
735 and Yutani, H. 2019. Welcome to the Tidyverse. J. Open Source Softw. **4**(43): 1686. The Open
736 Journal. doi:10.21105/JOSS.01686.

737 Williams, D.R., Epperson, L.E., Li, W., Hughes, M.A., Taylor, R., Rogers, J., Martin, S.L.,
738 Cossins, A.R., and Gracey, A.Y. 2005. Seasonally hibernating phenotype assessed through
739 transcript screening. Physiol. Genomics **24**(1): 13–22.
740 doi:10.1152/physiolgenomics.00301.2004.

741 Wood, S.H., Hindle, M.M., Mizoro, Y., Cheng, Y., Saer, B.R.C., Miedzinska, K., Christian,
742 H.C., Begley, N., McNeilly, J., McNeilly, A.S., Meddle, S.L., Burt, D.W., and Loudon, A.S.I.
743 2020. Circadian clock mechanism driving mammalian photoperiodism. Nat. Commun. **11**(1):
744 4291. doi:10.1038/s41467-020-18061-z.

745 Zavacki, A.M., Arrojo e Drigo, R., Freitas, B.C.G., Chung, M., Harney, J.W., Egri, P.,
746 Wittmann, G., Fekete, C., Gereben, B., and Bianco, A.C. 2009. The E3 Ubiquitin Ligase TEB4
747 Mediates Degradation of Type 2 Iodothyronine Deiodinase. Mol. Cell. Biol. **29**(19): 5339–
748 5347. doi:10.1128/MCB.01498-08.

749 Zhou, X., Lindsay, H., and Robinson, M.D. 2014. Robustly detecting differential expression in
750 RNA sequencing data using observation weights. Nucleic Acids Res. **42**(11): e91.
751 doi:10.1093/nar/gku310.

752

Figure legends

Figure 1: Photoperiod driven initiation and spontaneous termination of hibernation in golden hamsters (*Mesocricetus auratus*) relates to tanycyte transcriptional profile

A) Illustration of the experimental set-up and characteristic animal behaviour in response to shifting from long photoperiod 22°C (LP, 14 hours of light, 10 hours of dark) – summer like state, to short photoperiod (SP, 10 hours of light 14 hours of dark) and cold (8°C) – initiation of Autumn/Winter programme, followed by the eventual anticipation and initiation of Spring/Summer programme. Representative core body temperature (T_b) measurements are shown in parallel illustrate the physiological groups sampled in the experiment. T_b indicated in yellow relates to animals at LP 22°C, and T_b in blue relates to animals at SP 8°C. Ambient temperature (T_a) of the room is denoted by the grey dotted line. Pre-hib = Pre-hibernator 4 weeks after SP 8°C, Late pre-hib = pre-hibernator 8 to 12 weeks after SP 8°C, IBE = inter-bout euthermic. Hamster images were redrawn from https://commons.wikimedia.org/wiki/File:201606_hamster.png under the Creative Commons Attribution 4.0 International license. Attribution: DBCLS.

B) Mean euthermic core body temperature (T_b) throughout the experimental conditions. Each dot represents each individual mean euthermic T_b defined as each experimental group listed on the x-axis. For this analysis the refractory group was split into Refr. 0, 1 and 2 representing weeks after last torpor bout. Results of one-way ANOVA indicate a difference between the group mean T_b ($F_{(6, 45)} = 78.66$, $p<0.0001$). For **B, C, D, E** – The Tukey test determined the significant pairwise differences, indicated by different letters on the plot. LP = long photoperiod, pre-hib = Pre-hibernator 4 weeks after SP 8°C, L. pre-hib = pre-hibernator 8 to 12 weeks after SP 8°C, IBE = inter-bout euthermic, Refr. = refractory.

C) Each dot indicates each individual visible dissected interscapular brown adipose tissue (iBAT) mass in grams (y-axis) for the experimental groups (x-axis). Results of one-way ANOVA indicate a group mean difference in iBAT amount ($F_{(5,30)}$ =7.245, p<0.0001).

D) Each dot represents individual testes mass in grams for each experimental group at sampling. Results from one-way ANOVA indicate a difference between the group mean in testis mass ($F_{(5,30)}$=134.8, p<0.0001).

E) Blood plasma levels of testosterone. Each dot is each individual`s testosterone levels (ng/ml) for the experimental group indicated on the x-axis. Results from one-way ANOVA indicate a difference between the group mean in plasma testosterone levels ($F_{(5, 30)}$=25.91, p<0.0001).

F) Diagram to show the workflow from frozen whole brain through frozen cryosections to LASER Capture Microdissection (LCMD) of the ependymal layer of the tuberal part of the 3rd Ventricle (3V), which were further processed for Illumina RNA-seq.

G) Principal component analysis of differentially expressed genes (DEG) across the euthermic time points. The % variation contributing to each principle component (PC) are indicated on the x and y axis. The reproductively active animals, long photoperiod (LP) and refractory group together. The animals preparing for hibernation, pre-hibernation (pre-hib) and late pre-hibernation (late pre-hib) separate from the animals that have entered hibernation and are interbout euthermic, IBE). SP = short photoperiod.

Figure 2: Changes in ciliary genes and the glycolytic pathway in tanycytes defines the seasonal response to short photoperiod

A) Heatmap of seasonal DEGs (n= 2291) with k-means clustering into 5 clusters. Next to each cluster is a normalized counts per million (cpm) plot for all genes within each cluster to indicate direction of change between the groups as listed on the x-axis. Shown

as cluster mean normalised cpm (black line), shading ± Standard deviation and certain genes of interest color-coded as indicated.

B) Dot plot of enriched pathway for genes in the respective clusters using shinyGO analysis, both KEGG and reactome database results are shown. Size of dot represent number of genes. The colour of the dot represent -$\log_{10}$ transformed False discovery rate (*FDR*) value. The x-axis is the fold enrichment.

C) Specific GOterm enrichment for the genes in cluster 2. Size of dot represent number of genes. The colour of the dot represent -$\log_{10}$ transformed *FDR* value. The x-axis is the fold enrichment.

D) Cellular metabolic map of the glycolytic pathway, with the differentially expressed genes color-coded as indicated.

Figure 3: Increased immediate early gene expression and RNA splicing in the tanycytic region of torpid animals

A) Representative illustration of the core body temperature (T_b) recordings of an animal cycling from torpor to the interbout euthermic state and back again to torpor. Days spent in short photoperiod denoted on the x-axis.

B) Volcano plot for gene expression changes between interbout euthermic (IBE) and torpor. Dotted horizontal line indicate the false discovery rate, *FDR*= 0.05 threshold; Data are presented as $\log_2$ fold change, increased in inter bout euthermic (IBE) in red, increased in torpor in blue, genes with an *FDR*>0.05 are shown in green.

C) Counts per million plots across all samples for Fos, Wsb1, Eif5, Mlx. Each dot represents an individual count per million defined as each experimental group listed on the x-axis. A generalized linear model (GLM) analysis was used to assess the group mean gene expression differences (all genes had an *FDR* less than 0.0001); specific statistical values are in supplementary table 1.

D) Dot plot of enriched pathways for genes increased in torpor using shinyGO analysis, both Kyoto encyclopedia of genes and genomes (KEGG) and reactome database results are shown. Size of dot represent number of genes. The colour of the dot represent -$\log_{10}$ transformed *FDR* value. The x-axis is the fold enrichment.

E) Dot plot of enriched pathways for genes increased in interbout euthermic (IBE) using shinyGO analysis, both Kyoto encyclopedia of genes and genomes (KEGG) and reactome database results are shown. Size of dot represent number of genes. The colour of the dot represent -$\log_{10}$ transformed *FDR* value. The x-axis is the fold enrichment.

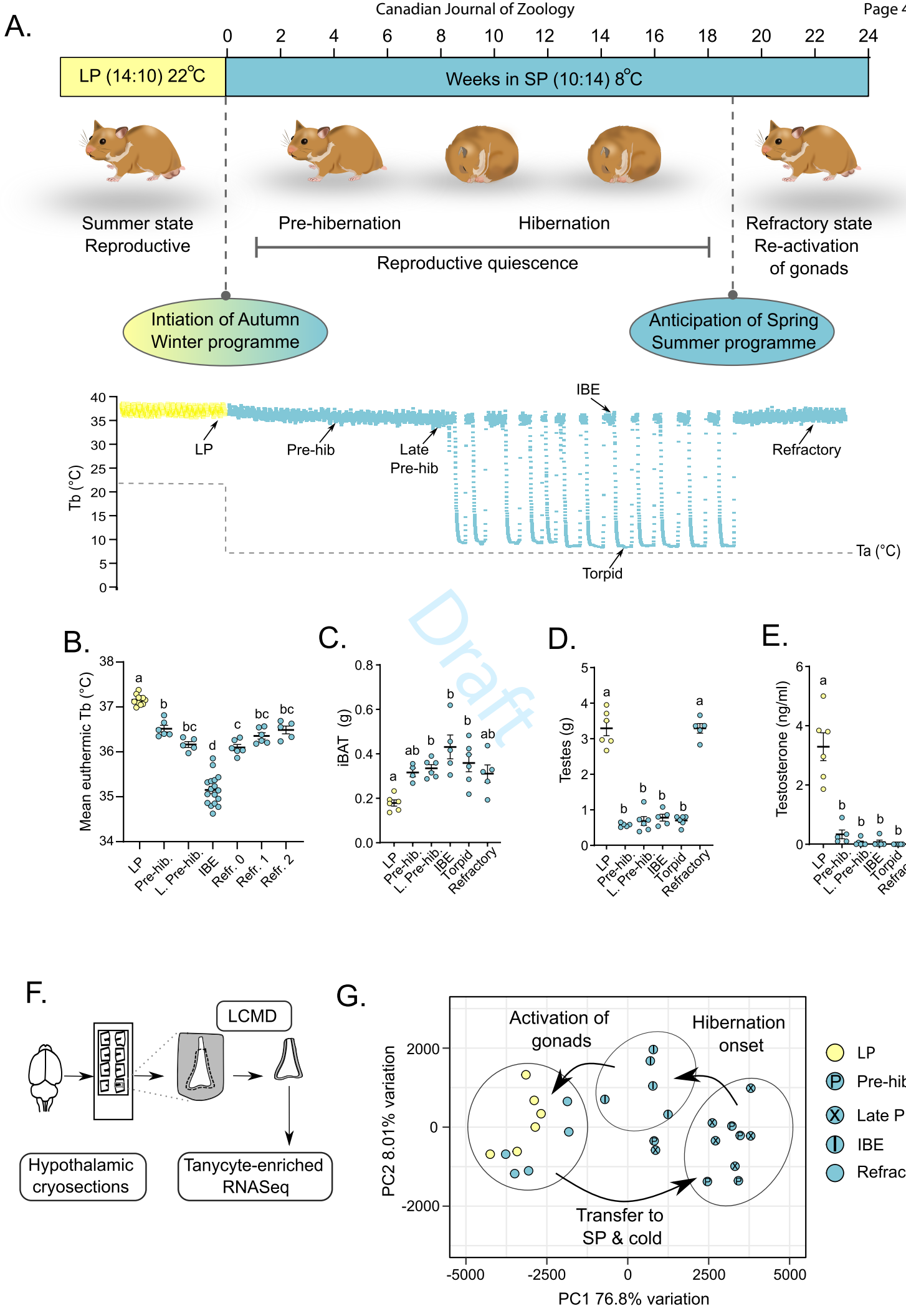

Figure 1

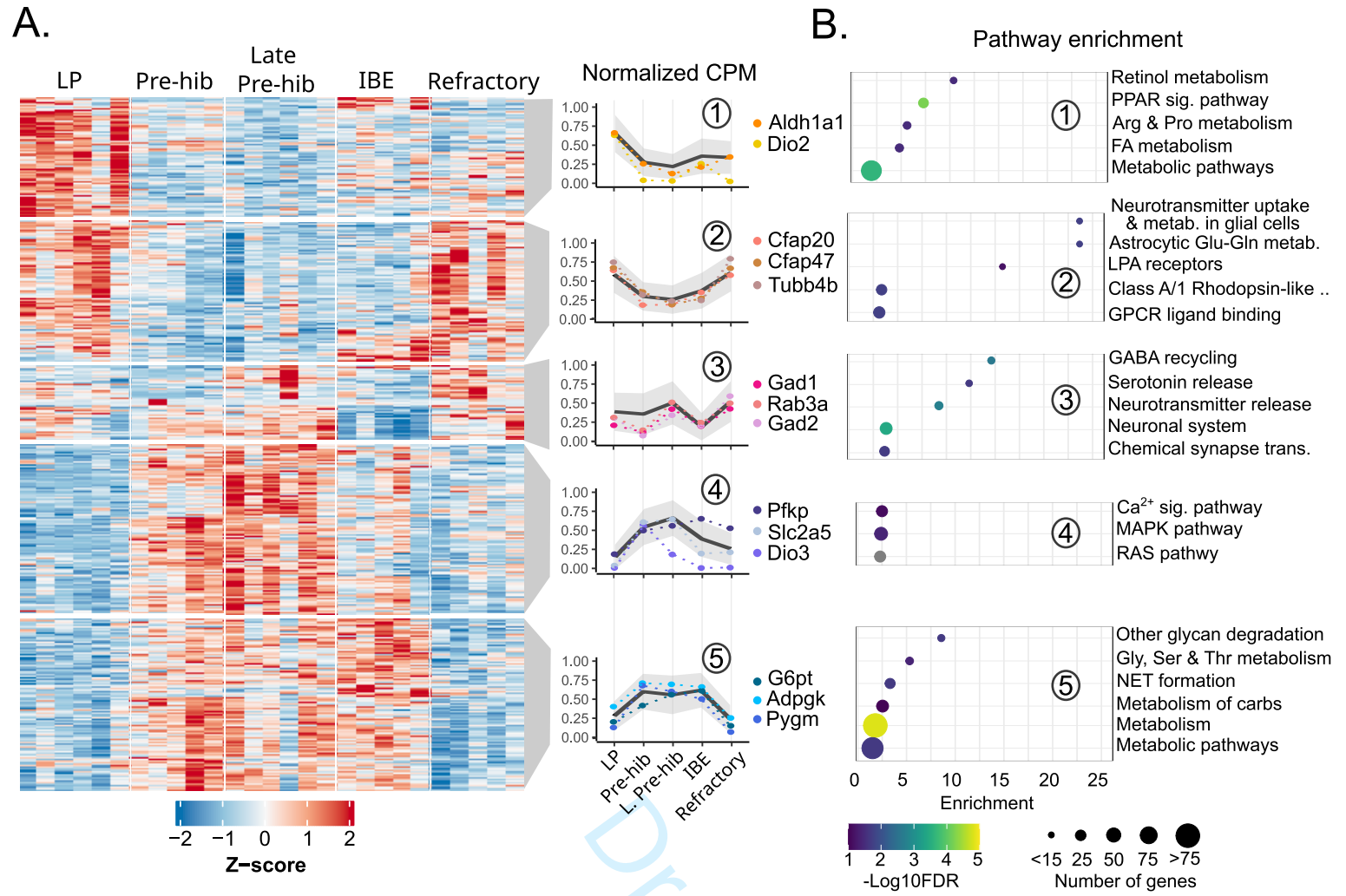

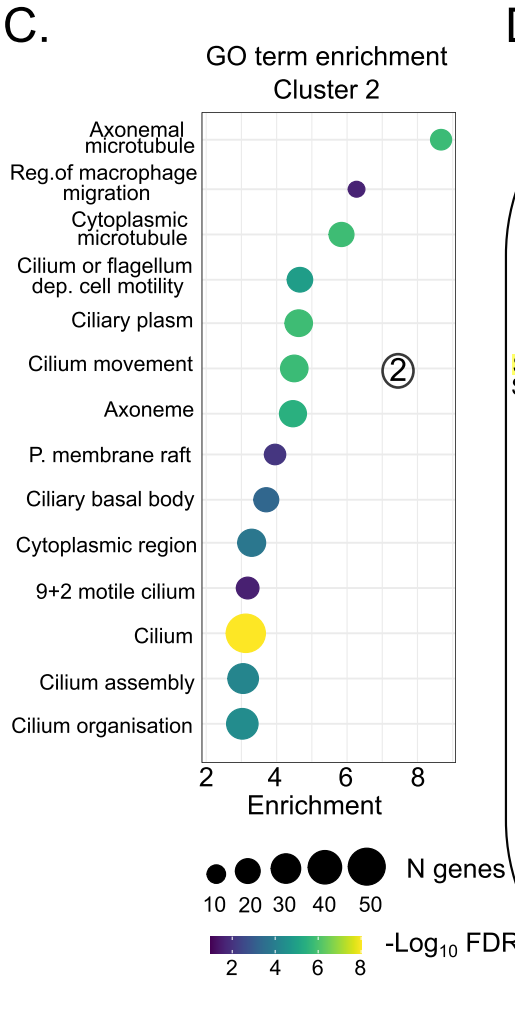

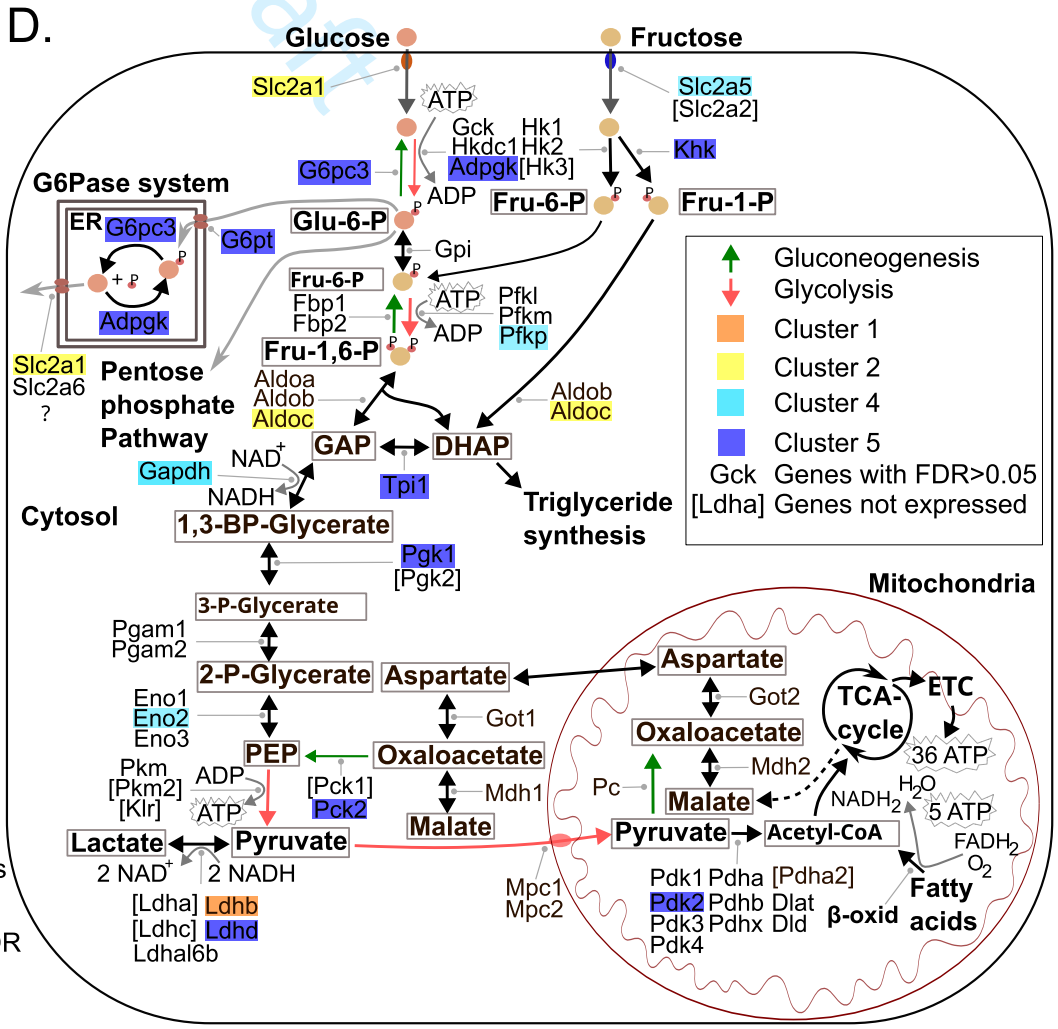

Figure 2

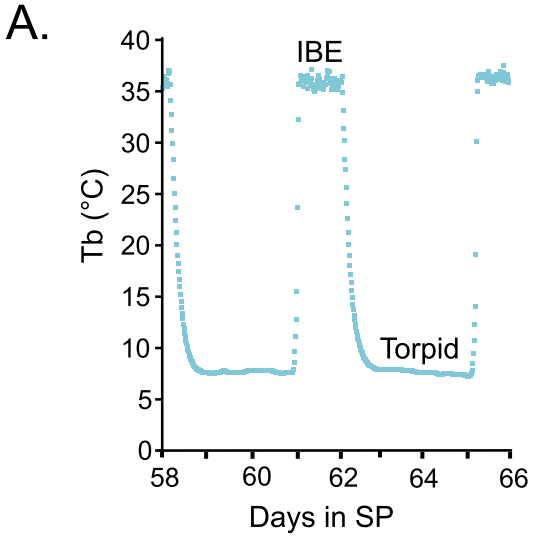

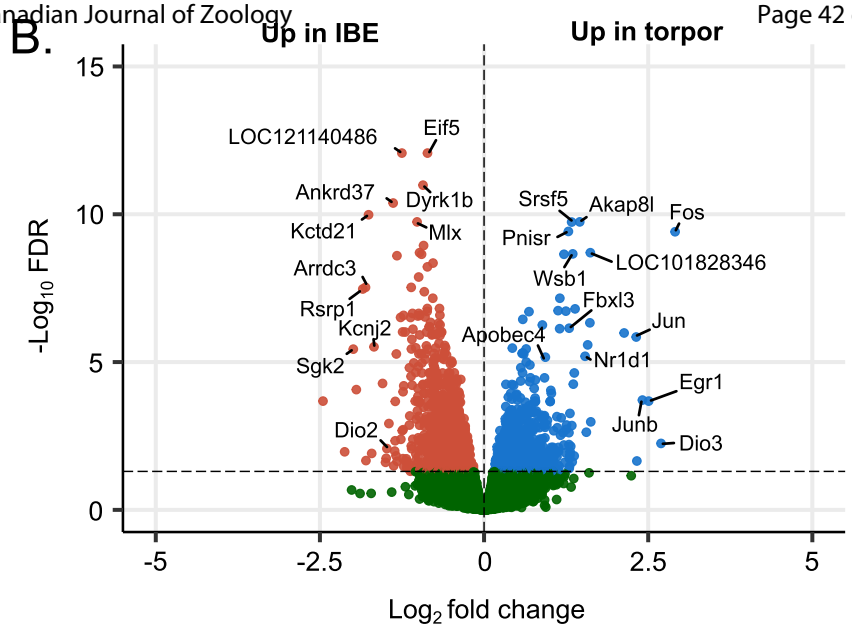

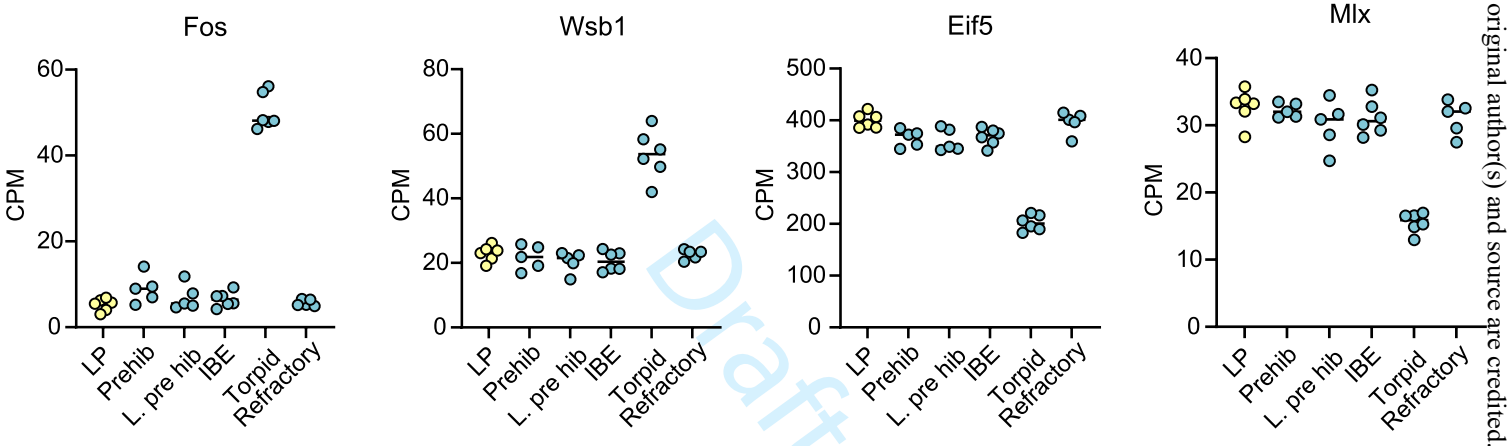

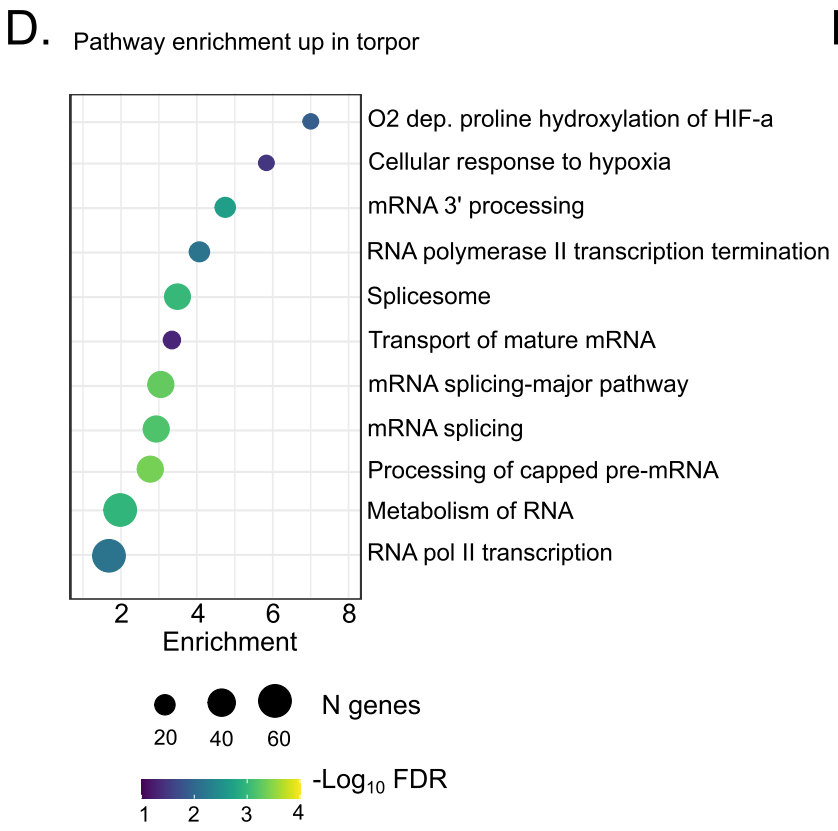

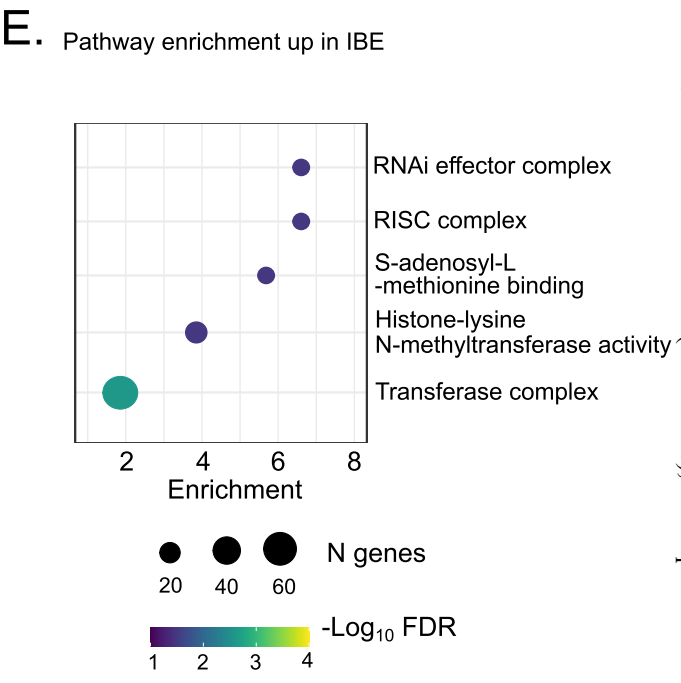

Figure 3